The Nature of the Mn Moment in Laves Phase Compounds: Evolution of the Magnetic Order in $Ho_{1-x}Y_xMn_2$

Clemens Ritter [1], Robert Cywinski [2], and Sue H. Kilcoyne [2,*]

[1] Institute Laue-Langevin, F-38042, Grenoble Cedex.
[2] J J Thomson Physical Laboratory, University of Reading, Reading RG6 2AF, UK

Z. Naturforsch. **50a**, 191–198 (1995); received September 26, 1994

Dedicated to Prof. Dr. W. Müller-Warmuth on the Occasion of his 65th Birthday

Neutron powder diffraction has been used to study the evolution of long range magnetic order in the pseudobinary C15 Laves phase system $Ho_{1-x}Y_xMn_2$. Particular attention has been paid to the nature of the Mn moment. At Y-rich compositions ($x>0.9$) an incommensurate antiferromagnetic structure, similar to that of YMn_2 is observed. Transition to the ordered state, as in YMn_2, is accompanied by a 5% expansion of the unit cell, identifying the Mn moments, of 2.7 μ_B, as intrinsic. The magnetic structure of compositions with $x<0.7$ resembles that of $HoMn_2$ and $DyMn_2$, with only one quarter of the chemically equivalent Mn sites possessing a moment of 0.6 μ_B induced by the local symmetry of the antiferromagnetically ordered Ho sublattice. Transition to the ordered state is not accompanied by a cell expansion. Between $x=0.7$ and $x=0.9$ there is no longe range magnetic order, nor is there an expansion of the unit cell, suggesting the total absence of either induced or intrinsic Mn moments. The results indicate that a critical Mn–Mn near neighbour distance of 2.663 Å is necessary to sustain an intrinsic Mn moment in these compounds.

Key words: $Ho_{1-x}Y_xMn_2$, Magnetic structure, Neutron diffraction, Laves phase.

Introduction

The magnetic ground state of manganese in the C14 and C15 Laves phase compounds RMn_2, where R is a 4f metal or Y, has been shown to depend sensitively on the Mn–Mn near neighbour distance, d_{Mn-Mn} [1]. At high temperatures ($T>100$ K) inelastic neutron scattering and μSR show the Mn magnetic moments to be in a spin fluctuating state [2]. With decreasing temperature those compounds with d_{Mn-Mn} larger then 2.66 Å develop an intrinsic moment at the Mn sites of approximately 2.8 μ_B [3]. The sudden appearance of this localised moment coincides with the onset of antiferromagnetic order and is accompanied by a marked increase in the volume of the unit cell. In the case of YMn_2 the volume anomaly, $\Delta V/V$, is as large as 5% [4]. In contrast, for those compounds with $d_{Mn-Mn}<2.66$ Å only some of the Mn sites develop a moment [5]. In this case the Mn moment is induced by a strongly polarising magnetic environment arising from the magnetically ordered 4f sublattice. For example, in cubic C15 $DyMn_2$ and $HoMn_2$ one in four of the chemically equivalent Mn sites possess an induced moment [5, 6]. The differences in character of the intrinsic and induced moments are underlined by the absence of a volume anomaly associated with the appearance of the latter.

Neutron powder diffraction, magnetostriction measurements and μSR have already been used to map the evolution from induced to intrinsic Mn moment in the pseudobinary system $Dy_{1-x}Y_xMn_2$ [7–10]. It has been shown that at intermediate concentrations, $0.7<1-x<0.3$, there is no longer range magnetic order. However, a volume anomaly of $\Delta V/V=1\%$ is observed at the "spin-glass" transition ($T_g=20$ K), providing evidence for the persistence of an intrinsic moment, of the order of 1 μ_B, throughout this magnetically disordered intermediate regime.

For $HoMn_2$ the Mn–Mn near neighbour distance is significantly smaller than that of $DyMn_2$. In principle, therefore, the pseudobinary series $Ho_{1-x}Y_xMn_2$ affords the possibility of exploring the transition from induced to intrinsic moment in more detail than does $Dy_{1-x}Y_xMn_2$. We have used neutron powder diffraction to study the phase diagram of cubic C15 $Ho_{1-x}Y_xMn_2$ in order to elucidate the interplay of structure and 4f metal interactions in defining the magnetic groundstate of Mn in the RMn_2 compounds.

* Present address: ISIS, Rutherford Appleton Laboratory, Chilton, OX11 0QX, UK.

Reprint requests to Dr. C. Ritter.

0932-0784 / 95 / 0200-0191 $ 06.00 © – Verlag der Zeitschrift für Naturforschung, D-72027 Tübingen

Experimental

Nine 15 gr samples from the $Ho_{1-x}Y_xMn_2$ series in the range $0 < x < 1$ were prepared by argon arc melting appropriate quantities of the constituent elements of purity better than 99.9% (Johnson-Matthey plc). A slight excess (5%) of Ho and Y over Mn was used to help suppress formation of the R_6Mn_{23} phase. The resulting ingots were subsequently powdered.

The neutron diffraction experiments were performed using the D1B high intensity powder diffractometer at the Institut Laue-Langevin (ILL), Grenoble. D1B uses a 2.52 Å monochromatic neutron beam and has a 400 element linear multidetector covering an angular range of 80°. The multidetector allows rapid data collection, typical diffraction patterns being accumulated in 10 minute intervals.

The powdered samples were contained in a vanadium can mounted in a standart ILL "orange" cryostat. Patterns were collected at temperatures between 2 K and 300 K. The resulting diffraction patterns were analysed using programs developed at the ILL. Individual Bragg peak intensities were determined using the ABFFIT programs, while full structural and magnetic profile refinement was carried out using a modified Rietveld method, FULLPROF [11, 12].

Results

The thermal evolution of the neutron diffraction patterns from four selected $Ho_{1-x}Y_xMn_2$ samples is shown in Figures 1–4. These patterns are characteristic of those obtained in four principle regions of the $Ho_{1-x}Y_xMn_2$ magnetic phase diagram, which is shown in Figure 5. These four regions will be discussed in turn below.

$0 < x < 0.35$

The thermogram in Fig. 1 is typical of those obtained from the Ho-rich samples with $x = 0.1$, 0.2 and 0.3. Initially antiferromagnetic Bragg peaks, associated with the AF2 structure, develop on cooling. On further cooling evidence for spin canting is provided by the appearance of a ferromagnetic (F) contribution at the nuclear Bragg peaks. The low temperature spectra could be fitted using the spin canted (AF2+F)

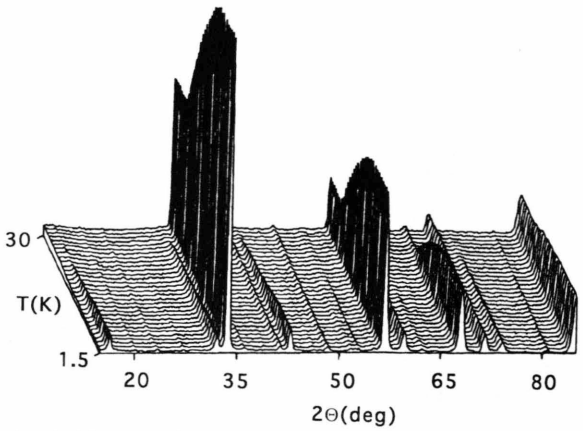

Fig. 1. Neutron thermogram of $Ho_{0.9}Y_{0.1}Mn_2$.

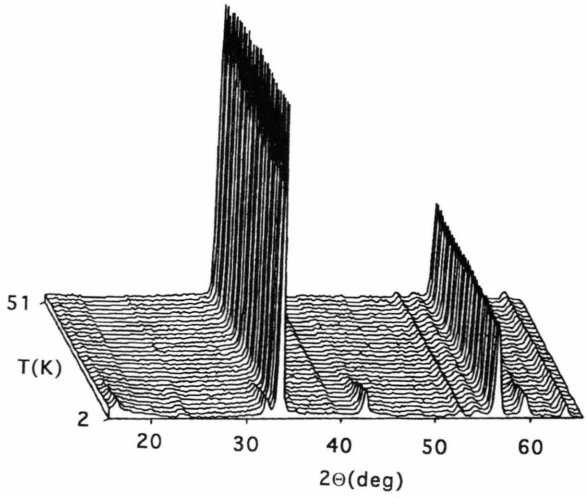

Fig. 2. Neutron thermogram of $Ho_{0.5}Y_{0.5}Mn_2$.

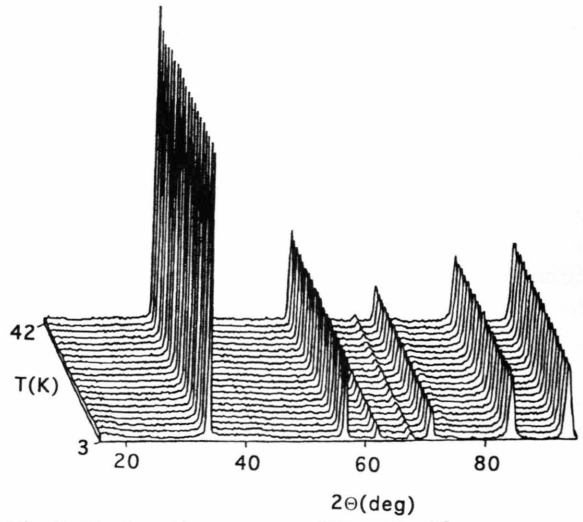

Fig. 3. Neutron thermogram of $Ho_{0.3}Y_{0.7}Mn_2$.

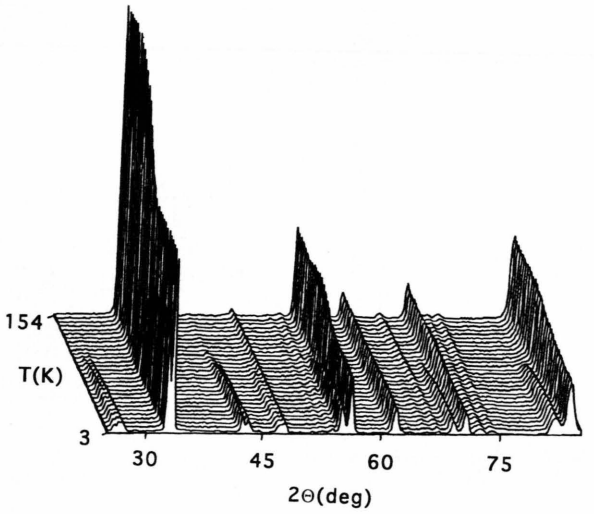

Fig. 4. Neutron thermogram of $Ho_{0.05}Y_{0.95}Mn_2$.

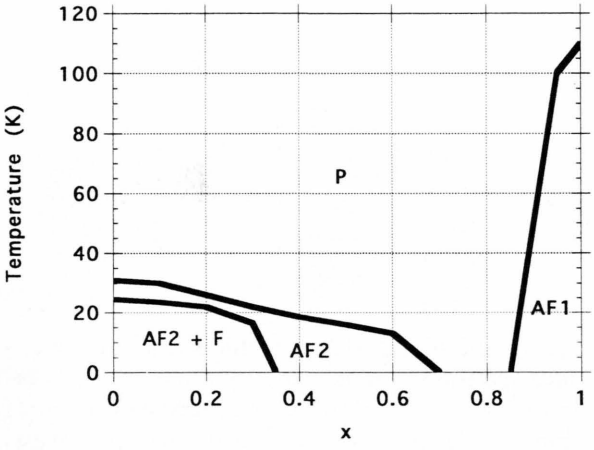

Fig. 5. The magnetic phase diagram of $Ho_{1-x}Y_xMn_2$. P stands for paramagnetic, AF1 and AF2 for antiferromagnetic order of first and second type for a cubic fcc lattice and F stands for ferromagnetism.

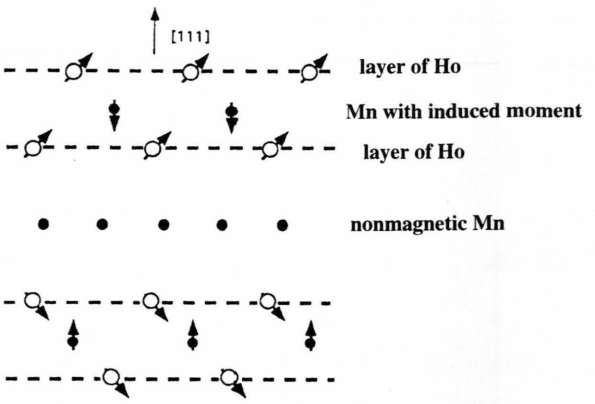

Fig. 6. The magnetic structure of $Ho_{1-x}Y_xMn_2$ with $0 \leq x < 0.65$. For more details see [5] and [8].

Table 1. Refined values of the magnetic moments in $Ho_{1-x}Y_xMn_2$ tabulated as function of $1-x$. F and AF stand for ferro- and antiferromagnetic component of the rare earth sublattice. F_{corr} and AF_{corr} are values corrected for the actual Ho concentration and give the values per Ho atom. Mn stands for Manganese moment. All values are in units of μ_B.

$1-x$	F	F_{corr}	AF	AF_{corr}	Mn
0.3	–	–	–	–	–
0.4	–	–	1.17 (6)	2.93 (15)	0.2 (1)
0.5	–	–	2.25 (5)	4.50 (10)	0.25 (10)
0.6	–	–	3.72 (5)	6.20 (8)	0.55 (7)
0.7	2.89 (9)	4.13 (13)	3.82 (6)	5.45 (9)	0.65 (6)
0.8	4.93 (13)	6.16 (16)	3.62 (15)	4.53 (19)	0.63 (10)
0.9	6.07 (16)	6.74 (18)	3.00 (18)	3.33 (20)	0.52 (13)
1.0	7.03 (20)	7.03 (20)	3.46 (21)	3.46 (21)	0.62 (20)

structure reported previously for the pure $DyMn_2$ and $HoMn_2$ [5, 6] compounds and illustrated in Figure 6. Increasing the substitution of nonmagnetic Y leads to a decrease in the magnitude of the ferromagnetic component (and hence in the spin canting) whilst the antiferromagnetic component is little changed (Table 1). As it is the antiferromagnetic component of the 4f-metal spin structure that is responsible for the exchange induced magnetic moment at one in four of the Mn sites, the magnitude of the induced Mn moment remains constant at 0.6 μ_B. "Curie" and Néel temperatures have been determined from the variation of the magnetic Bragg intensities with temperature. Both decrease with increasing Y substitution. Table 1 summarises the principal magnetic parameters obtained from refinement of the magnetic structures, together with the previously reported values for $HoMn_2$.

Sequential refinement of the lattice parameter was performed for all three samples in this concentration regime. Although the thermal expansion coefficient (TEC) above T_N is moderately enhanced ($TEC = 27 \times 10^{-6}\ K^{-1}$) indicative of spin fluctuating 3d moments, there is no sign of a volume anomaly at T_N for any of the samples.

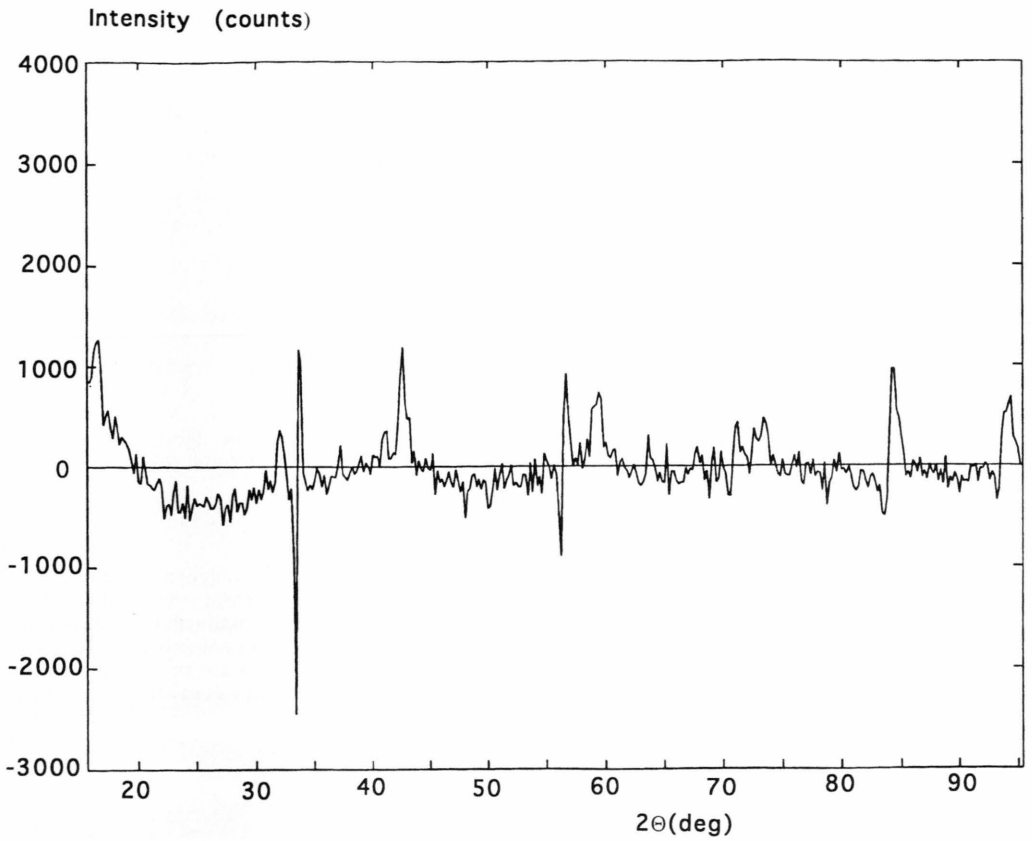

Fig. 7. The 30 K–2 K difference pattern of $Ho_{0.4}Y_{0.6}Mn_2$.

$0.35 < x < 0.65$

This range of the magnetic phase diagram is characterised by the disappearance of the ferromagnetic component of the spin structure of the rare earth sublattice. The antiferromagnetic coupling persists, however, as can be seen in the thermogram of $Ho_{0.5}Y_{0.5}Mn_2$ (Figure 2). The values of the magnetic moments and ordering temperatures extracted from refinement of the diffraction patterns are listed in Table 1.

$Ho_{0.6}Y_{0.4}Mn_2$ sees an AF2 coupling comparable to that of the Ho-rich samples discussed above, and consequently the induced Mn moment on every fourth site remains constant at 0.6 μ_B. However, further dilution by Y decreases the 4f-metal exchange coupling and hence the magnitude of the Mn moments. Figure 7 shows the difference between $Ho_{0.4}Y_{0.6}Mn_2$ spectra collected at 2 K and 30 K. While AF2 antiferromagnetic Bragg peaks are still evident, the difference spectrum is dominated by a modulated background arising from massive magnetic short range 4f spin correlations associated with the AF2 phase. Statistics are not sufficient to analyse this magnetic short range order quantitatively doing a Fourier transform analysis. As a rough estimate an upper limit for the correlation length of 30 Å can be determined using the Scherrer formula for peak broadening [13].

Again, in this concentration range, sequential refinement of the structural parameters shows no volume anomaly at T_N. A TEC of $29 \times 10^{-6}\ K^{-1}$ is obtained.

$0.65 < x < 0.85$

The thermogram of $Ho_{0.3}Y_{0.7}Mn_2$ (Fig. 3) shows no evidence of long range magnetic order down to

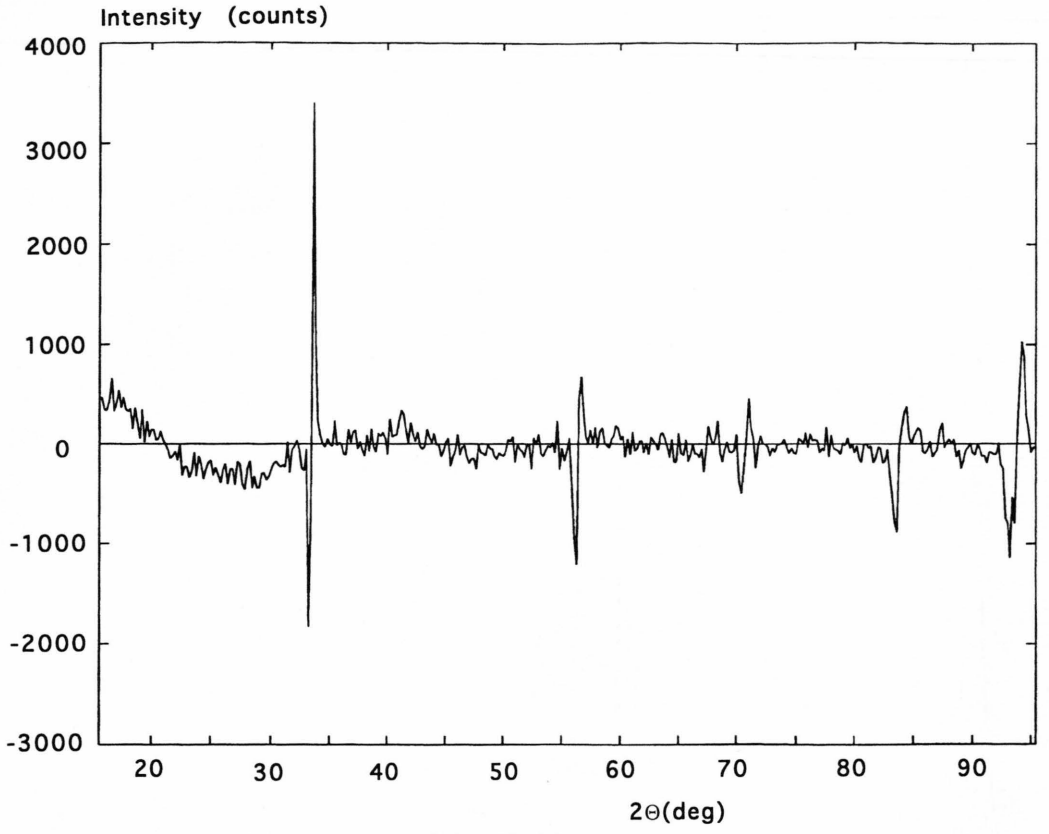

Fig. 8. The 30 K – 5 K difference pattern of $Ho_{0.3}Y_{0.7}Mn_2$.

2 K. The difference plot, 5 K – 30 K, for this compound (Fig. 8) provides evidence of persisting AF2 correlations, with a correlation length of again less than 30 Å. The antiferromagnetic Dy–Dy correlations are therefore of considerably shorter range than those observed in the "nonmagnetic" state at intermediate concentrations of the $Dy_{1-x}Y_xMn_2$ series where they amounted to about 100 Å [8]. Also in contrast to the $Dy_{1-x}Y_xMn_2$ compounds, sequential refinement of the $Ho_{0.3}Y_{0.7}Mn_2$ spectra shows no volume anomaly at any temperature.

$0.85 < x < 1$

Figure 4 shows the neutron thermogram obtained from the $Ho_{0.05}Y_{0.95}Mn_2$ sample. The principal features of the thermogram are similar to those found in most dilute rare earth substituted YMn_2 compounds. There is a transition to antiferromagnetic order close to $T_N = 100$ K, which is accompanied by a massive thermal expansion anomaly. In this compound, however, only 34% of the sample transforms to the expanded antiferromagnetic phase, the remaining volume fraction staying paramagnetic. This results in an apparent decrease of the peak intensity of the nuclear Bragg peaks as the intensity is distributed between split nuclear peaks below T_N.

In Fig. 9 the spectrum obtained from $Ho_{0.05}Y_{0.95}Mn_2$ at 2 K is shown. The split nuclear peaks reveal the coexistence of the expanded and nonexpanded phases. The antiferromagnetic Bragg peaks are worthy of closer inspection: at low angles where the resolution of the D1B diffractometer is optimal, one can clearly distinguish a splitting of these peaks. The first three magnetic peaks at $2\Theta = 31°$, 42° and 47° can be indexed, using the AF1 model proposed for YMn_2 [14], as 110, 201 and 112. For YMn_2 a propa-

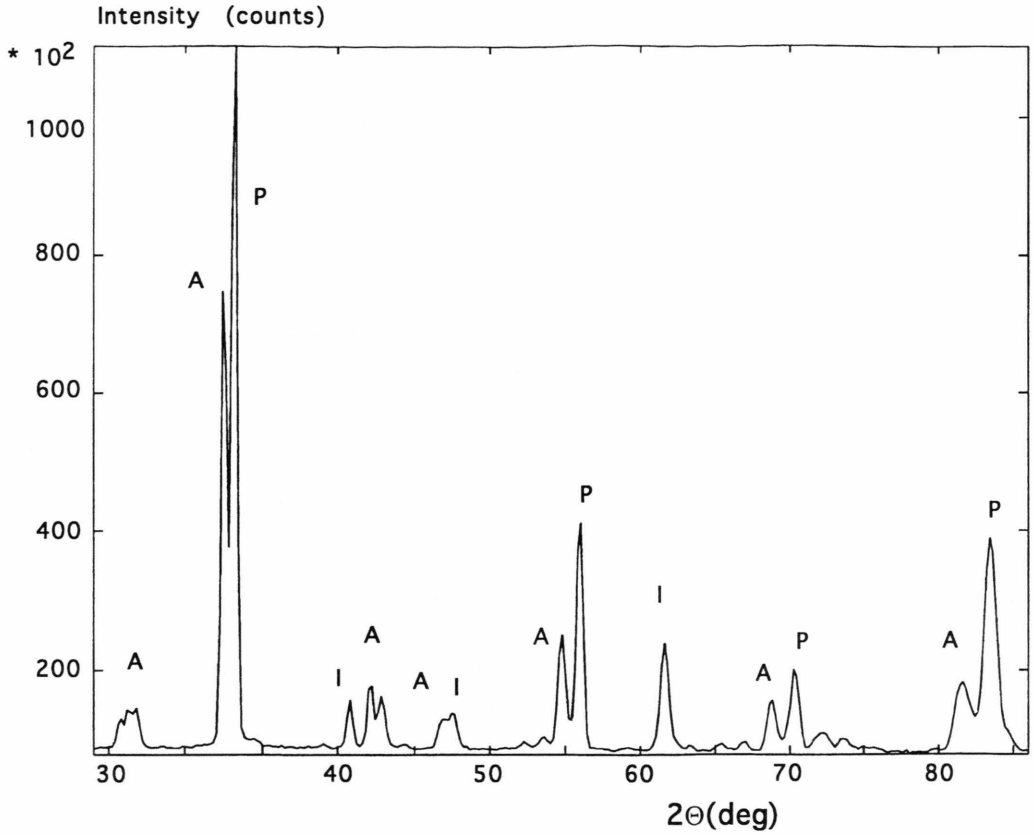

Fig. 9. The 2 K neutron diffraction pattern of $Ho_{0.05}Y_{0.95}Mn_2$. A stands for antiferromagnetic phase, P for paramagnetic phase and I for impurity phase.

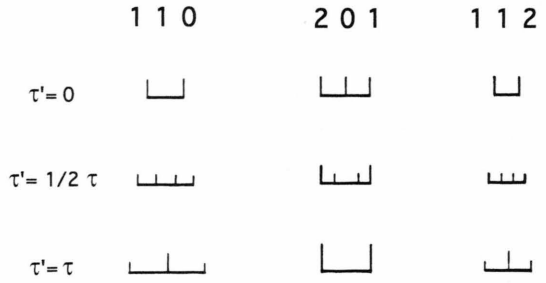

Fig. 10. A schematic presentation of the influence of the second component τ' of the propagation vector $[\tau\tau'1]$ on the splitting of the first 3 antiferromagnetic reflections in $Ho_{0.05}Y_{0.95}Mn_2$.

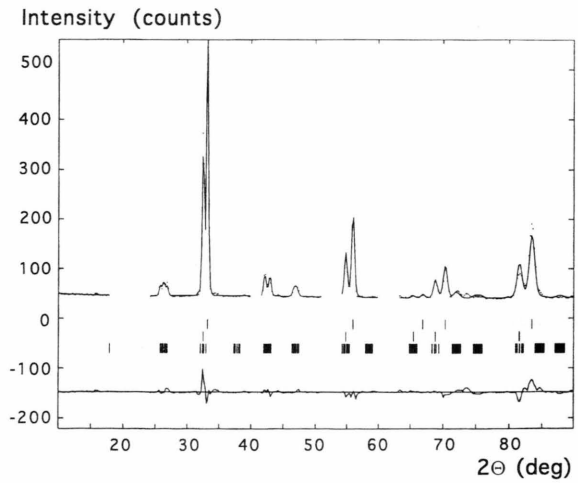

Fig. 11. The observed, calculated and difference powder neutron diffraction profils of $Ho_{0.05}Y_{0.95}Mn_2$ at 2 K using a propagationvector $[\tau\tau'1]$.

gation vector [$\tau\tau'1$], with $\tau = 0.018$ and $\tau' = 0.003$ has been determined from high resolution powder diffraction measurements [15]. In $Ho_{0.05}Y_{0.95}Mn_2$ the observed splitting of the magnetic peaks, and hence the magnitude of the τ-vectors, have significantly increased.

In Fig. 10 we explain schematically the influence of the two incommensurate components of the propagation vector on the splitting of the 110, 201 and 112 reflections: in particular note that when $\tau = \tau'$ three peaks are observed at the 110 position while two peaks are found at 201. Using a modified Rietveld program which allows the refinement of incommensurate magnetic structures we obtain for $Ho_{0.05}Y_{0.95}Mn_2$ at 2 K the propagation vector [$\tau\tau'1$], with $\tau = 0.024$ and $\tau' = 0.015$ (Figure 11).

It can be seen in Fig. 4 that the shape of the 110 peak evolves with temperature. A sequential Rietveld refinement of the temperature dependent magnetic structure of $Ho_{0.05}Y_{0.95}Mn_2$ provides the components of the propagation vector shown in Figure 12. While τ remains almost constant at 0.023(1), τ' decreases significantly from 0.015 at 2 K to 0.0065 at 83 K.

The value of the Mn moment in the expanded antiferromagnetic phase is 2.6(1) μ_B at 2 K and 2.75(15) μ_B at 83 K, at which temperature only 12% of the sample volume is still in the expanded phase.

Refining the cubic lattice parameters a volume expansion of $\Delta V/V = 5.8\%$ is observed on cooling into the antiferromagnetic phase. This identifies the Mn moment as intrinsic. Correspondingly, in the paramagnetic phase, we find TEC $= 53 \times 10^{-6}\ K^{-1}$. This

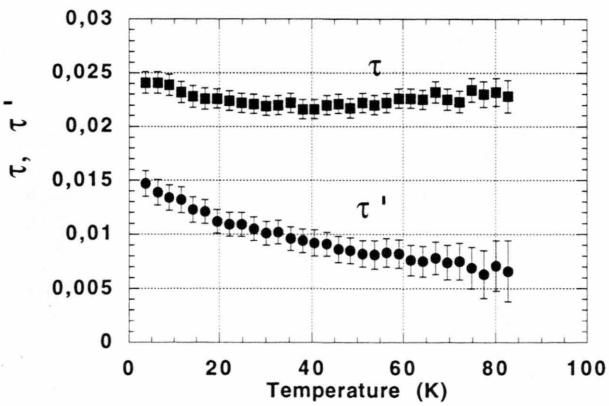

Fig. 12. Temperature dependence of the components τ and τ^* of the incommensurate propagation vector $\varkappa = [\tau\tau^*1]$ of $Ho_{0.05}Y_{0.95}Mn_2$.

Table 2. Results of the refinement for the Y-richest phases. a_0 para and a_0 anti stand for the cubic lattice parameters in the para- and antiferromagnetic part of the sample volume at 2 K.

	$Ho_{0.1}Y_{0.9}Mn_2$	$Ho_{0.05}Y_{0.95}Mn_2$
μ_{Mn}	2.65 (35) μ_B	2.6 (1) μ_B
$\Delta V/V$	4.7%	5.8%
a_0 para	7.535 (95%)	7.543 (66%)
a_0 anti	7.652 (5%)	7.686 (34%)
TEC	$40 \times 10^{-6}\ K^{-1}$	$53 \times 10^{-6}\ K^{-1}$

value, like that of the parent compound YMn_2 is anomalously high, and is consistent with a spin fluctuating state above T_N.

For the $Ho_{0.1}Y_{0.9}Mn_2$ sample only a transformation to the expanded antiferromagnetic state is observed at $T_N = 60$ K. The magnetic structure is little changed from that of $Ho_{0.05}Y_{0.95}Mn_2$, with the Mn moment refining to 2.65(15) μ_B. The volume anomaly at T_N is $\Delta V/V = 4.7\%$ which is still very large and comparable to that of pure YMn_2. The principal results obtained from the refinement of the two Y-rich samples are summarized in Table 2. It should be noted that there is no evidence of the participation of Ho moments in the observed AF1 phase.

Discussion and Conclusions

The pseudobinary C15 Laves phase system $Ho_{1-x}Y_xMn_2$ reveals a magnetic phase diagram which embraces a transition from a large ($\mu_{Mn} = 2.7\ \mu_B$) intrinsic localised Mn moment at high Y concentrations ($x > 0.9$) to a small ($\mu_{Mn} = 0.6\ \mu_B$) induced Mn moment at one in four of the Mn sites at intermediate and high Ho concentrations ($x < 0.7$).

The transition between these two extremes does not proceed via a broad intermediate state characterised by disordered intrinsic Mn moments, as observed in the case of the related $Dy_{1-x}Y_xMn_2$ system [7]. Instead $Ho_{1-x}Y_xMn_2$ shows a relatively narrow disordered region ($0.7 < x < 0.9$) in which there is no evidence for either intrinsic or induced moments at the Mn sites.

The apparent absence of Mn moments in this disordered region enabled us to determine accurately a critical Mn–Mn distance above which an intrinsic Mn moment can be formed. We obtain $d_c = 2.663$ Å, in very close agreement with the value extracted from our study of the $Dy_{1-x}Y_xMn_2$ phase diagram [8].

The existence of long range AF2-type magnetic order of the rate earth sublattice down to $Ho_{0.04}Y_{0.6}Mn_2$ gives a strong indication of the important role R-Mn interactions play in the case of the $Dy_{1-x}Y_xMn_2$ series [7, 8]. There, in the presence of a small intrinsic moment on Mn, only short range order is preserved on the Dy sublattice for $x > 0.3$.

Although intrinsic moments cannot form for $d_{Mn-Mn} < d_c$, the large TEC found in the paramagnetic phase at all compositions indicates presence of a spin fluctuating Mn moment, possibly close to localisation, to well below the critical distance.

The magnetic structure of the YMn_2 samples with dilute Ho substitution is rather enigmatic: for dilute Tb and Dy substitution a commensurate AF1 phase is observed [7, 16].

It has been suggested that in pure YMn_2 the magnetic frustation resulting from the superposition of antiferromagnetic order upon a tetrahedral Mn-site topology gives rise to both a tetragonal distortion of the unit cell and an incommensurate magnetic structure [15, 17]. For Tb and Dy substitution in YMn_2 it appears that for these substituents at least, the magnetic frustration can be relieved without recourse to incommensurability: diffraction studies of these compounds have not yet been performed at sufficiently high resolution to assess the role of any tetragonal distortion.

We might speculate that in the case of Ho substitution the tetragonal distortion of the lattice below T_N is suppressed, leaving incommensurability as the only route by which the magnetic frustration can be relieved. Such speculation can only be resolved with further, high resolution, neutron diffraction measurements.

[1] M. Shiga, Physica B **149,** 293 (1988).
[2] B. D. Rainford, S. Dakin, R. Cywinski, J. Magn. Magn. Mater. **104–107,** 1257 (1992).
[3] B. Ouladdiaf, Thesis Grenoble 1986.
[4] Y. Nakamura, J. Magn. Magn. Mater. **31–34,** 829 (1983).
[5] C. Ritter, S. H. Kilcoyne, and R. Cywinski, J. Phys: Condens. Matter **3,** 727 (1991).
[6] C. Ritter, S. Mondal, S. H. Kilcoyne, and R. Cywinski, J. Phys: Condens Matter **4,** 1559 (1992).
[7] C. Ritter, S. Mondal, S. H. Kilcoyne, R. Cywinski, and B. D. Rainford, J. Magn. Magn. Mater. **104–107,** 1427 (1992).
[8] C. Ritter, R. Cywinski, S. H. Kilcoyne, S. Mondal, and B. D. Rainford, Phys. Rev. B **50,** 9894 (1994).
[9] C. Ritter, C. Marquina, and M. R. Ibarra, sub. J. Magn. Magn. Mater.
[10] M. Telling, R. Cywinski, S. H. Kilcoyne, and C. Ritter, to be published.
[11] A. Filhol, J. Y. Blanc, A. Anoniadis, and J. Berruyer, Institut Laue-Langevin Report 88FI05T (1988).
[12] J. Rodriguez-Carvajal, M. Anne, and J. Pannetier, Institut Laue-Langevin Report 87RO114T (1987).
[13] C. Legrand, Bull. Soc. Fr. Cer. **95,** 101 (1972).
[14] T. Freltoft, B. Boni, G. Shirane, and K. Motoya, Phys. Rev. B **37,** 3454 (1988).
[15] R. Cywinski, S. H. Kilcoyne, and C. A. Scott, J. Phys: Condens. Matter **3,** 6473 (1991).
[16] R. Ballou, J. Deportes, R. Lemaire, R. Rouault, and J. L. Soubeyroux, J. Magn. Magn. Mater. **90–91,** 559 (1990).
[17] R. Ballou, J. Deportes, R. Lemaire, Y. Nakamura, and B. Ouladdiaf, J. Magn. Magn. Mater. **70,** 129 (1987).